Int J Earth Sci (Geol Rundsch) (2017) 106:1359–1373
DOI 10.1007/s00531-016-1373-5

ORIGINAL PAPER

Late Triassic post-collisional slab break-off along the Ailaoshan suture: insights from OIB-like amphibolites and associated felsic rocks

Huichuan Liu[1] · Yuejun Wang[1] · Xiaofei Guo[2] · Weiming Fan[2] · Jingjing Song[2]

Received: 8 March 2016 / Accepted: 6 July 2016 / Published online: 1 August 2016

Abstract What dynamic processes the South China-Indochina collision had gone through is still a pending problem. Our recent investigations identified a Late Triassic gabbroic intrusion in Mengdong village and several granitic plutons near Wana village, Yunnan province (SW China). Both have underwent strong metamorphism and been altered to amphibolite and granitic gneiss, respectively. We carried out SIMS and LA-ICPMS zircon U–Pb dating for the amphibolites and granitic gneisses, respectively. Dating results yield weighted mean $^{206}Pb/^{238}U$ ages of 221.5 ± 5.3 Ma for the amphibolites and 224.0 ± 1.8 and 235.4 ± 0.6 Ma for the granitic gneisses. The amphibolite samples have low $Mg^{\#}$ (41.7–42.8), high TiO_2 (~3.7 wt%) and Na_2O (Na_2O/K_2O = 1.89–2.68) contents and depleted Sr–Nd isotopic compositions [$(^{87}Sr/^{86}Sr)i$ = 0.707647 and $\varepsilon_{Nd}(t) = +1.17$]. They exhibit OIB-like REE patterns and spidergrams, with strongly enriched LREE contents, insignificant Eu anomalies (Eu* = 0.99–1.03) and moderate negative Sr anomalies (Sr* = 0.46–0.56). The protolith gabbro of the Mengdong amphibolites is derived from low-degree partial melting of a homogeneous OIB-type mantle source in the garnet stability field and experienced significant fractionation of olivine, clinopyroxene and plagioclase during magma evolution. The Wana samples are strongly peraluminous (A/CNK > 1.1) and K-enriched (K_2O/Na_2O = 2.93–3.63). They show enriched Sr–Nd isotopic compositions with $(^{87}Sr/^{86}Sr)i$ = 0.718589–0.719754 and $\varepsilon_{Nd}(t) = -11.34$ to -10.92. The Wana plutons are typical S-type granite and product of the dehydration melting of meta-sedimentary rocks. We summarized Late Triassic age data in the literature along the South China-Indochina suture zone and recognized a significant Late Triassic magmatic flare-up. In combination with previous studies on the Late Triassic HP–UHP metamorphic rocks, we proposed that during the Late Triassic the South China-Indochina suture zone had transformed into post-collisional setting, and accompanied slab break-off triggered the OIB-type asthenospheric mantle upwelling and provided the heat source for the Late Triassic magmatic flare-up.

Keywords Indosinian Orogeny · Slab break-off · Paleotethys · OIB · Post-collision

Introduction

Slab break-off has been suggested to occur locally during the subduction of young plate, mid-ocean ridge and mature oceanic lithosphere (e.g., Levin et al. 2002; Schoonmaker et al. 2005; Tang et al. 2012), but most usually following the continental collision (e.g., Atherton and Ghani 2002; Davies and Von Blanckenburg 1995; Gulmez et al. 2013). In continental collision setting, the eclogitized slab break-off may induce asthenosphere upwelling and subducted continental crust rebounding, producing the partial melting of the overlying lithospheric mantle and crust (e.g., Xu et al. 2000), and the followed asthenosphere upwelling will trigger the extension and/or rifting of the overlying crust.

Electronic supplementary material The online version of this article (doi:10.1007/s00531-016-1373-5) contains supplementary material, which is available to authorized users.

✉ Yuejun Wang
wangyuejun@mail.sysu.edu.cn

[1] Present Address: School of Earth Science and Geological Engineering, Sun Yat-Sen University, Guangzhou 510275, China

[2] CAS Center for Excellence in Tibetan Plateau Earth Sciences, Beijing 100101, China

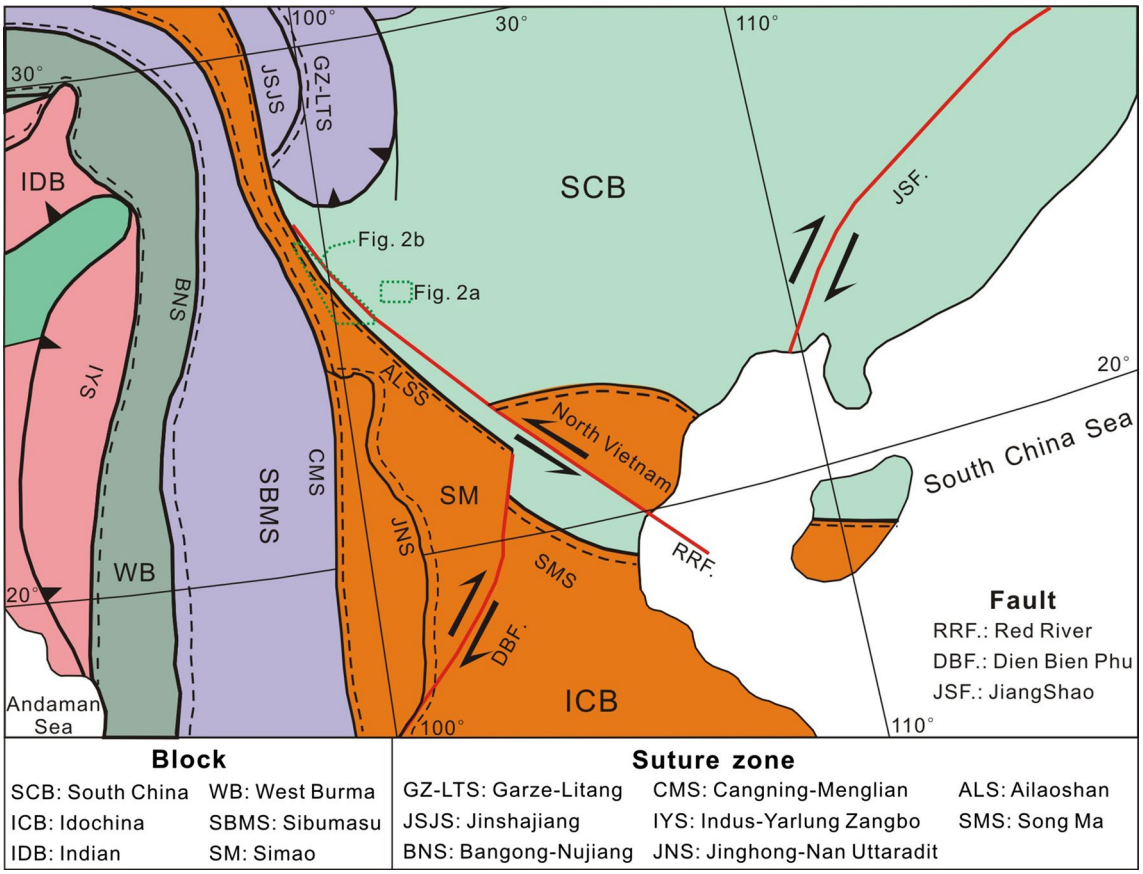

Fig. 1 Tectonic outline of Southeast Asia (revised from Cai and Zhang 2009; Metcalfe 2013; Wang et al. 2013)

In SE Aisa, the closure of the Paleotethyan branch ocean along the notable NW-trending Jinshajiang–Ailaoshan–Song Ma (JAS) suture zone leads to the collision of the South China with Indochina blocks during Late Permian to Late Triassic (Fig. 1; Liu et al. 2015; Metcalfe 2013; Yang et al. 2014). This event has been recognized as the Indosinian Orogeny marked stratigraphically by the unconformity between Upper Triassic red beds and deformed Middle Triassic and older metamorphic rocks in northern Vietnam and southwestern China (Deprat 1914; Lepvrier et al. 2008). The Indosinian Orogeny has been recorded in a large region including the whole Indochina peninsula, eastern Tibet and South China (Chen et al. 2011; Lacassin et al. 1998). Multiple collisions in SE Asia during the Permian–Triassic are linked to the Indosinian Orogeny, and a three-phase evolutionary model has been proposed for the Indosinian Orogeny (Lepvrier et al. 2008; Sone and Metcalfe 2008; Liu et al. 2015; Zi et al. 2013). However, due to the strong Cenozoic structural overprinting, collisional-related igneous rocks, especially the mafic components which are an effective indicator for probing the mantle nature, are poorly exposed, thus resulting into the queries on the orogenic dynamics of the Indosinian event.

Our investigations identified Late Triassic gabbroic and granitic plutons nearby the Mengdong village (Malipo county, Yunnan province; Fig. 2a) and Wana village (Yuanjiang county, Yunnan province; Fig. 2b), respectively. They have underwent strong metamorphism and been altered to amphibolite and granitic gneiss. In this study, we conducted zircon U–Pb geochronological, whole-rock elemental and Sr–Nd isotopic analyses for the Mengdong amphibolite and Wana granitic gneiss samples. Our new data suggest that the Mengdong amphibolite is OIB-like and the Wana granitic gneiss shows geochemical characteristics of S-type granite. These data, together with the Late Triassic high $\varepsilon_{Nd}(t)$–$\varepsilon_{Hf}(t)$ I-type granite (Liu et al. 2014), the pelitic granulite in the Ailaoshan belt (Qi et al. 2012), the mafic granulite (Nakano et al. 2008) and eclogite (Nakano et al. 2010; Zhang et al. 2013) in northern Vietnam, allow us to evaluate the collisional mechanism of the Indosinian Orogeny.

Geological background

SE Asia is composed of three major tectonic blocks: South China, Simao-Indochina and Sibumasu (Fig. 1). Two pairs

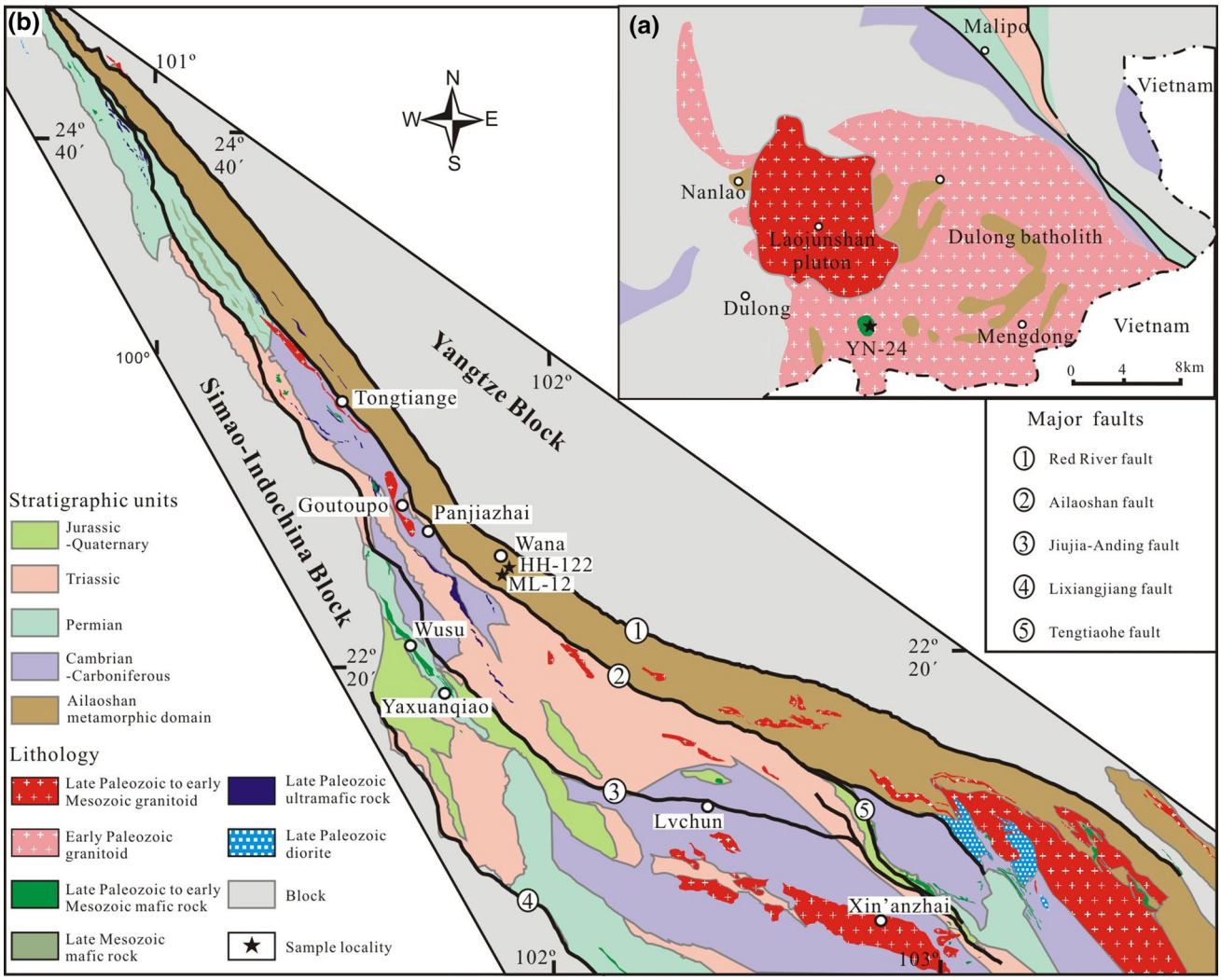

Fig. 2 Geological map showing the stratigraphic sequences and igneous rocks of the Dulong (**a**) and Ailaoshan (**b**) areas (modified from YunnanBGMR 1990)

of sutures, the Jinshajiang–Ailaoshan–Song Ma (JAS) suture and Changning–Menglian–Inthanon (CMI) suture, were formed due to the closure of the Paleotethyan oceans (Fig. 1; Lai et al. 2014a; Metcalfe 2013; Zhang et al. 2014b). The South China block is separated by the JAS suture from the Simao-Indochina block to the west. The Simao-Indochina block is limited by the CMI suture to its west and by the JAS suture to the east (Fig. 1). The age distribution patterns of pre-Carboniferous detrital zircons from Indochina blocks are more similar to those from the Greater India than to those from the western part of the South China block (Usuki et al. 2013), and thus the Simao-Indochina block was derived from the Indian Gondwana instead of the South China block. Mid-Neoproterozoic arc magmatism in the Ailaoshan complexes and the Mid-Neoproterozoic HP metamorphic rocks in the North Lhasa terrane marked that the Yangtze and Simao-Indochina blocks amalgamated in the Mid-Neoproterozoic (860–730 Ma; Qi et al. 2014; Wang et al. under review). After that, the Proterozoic metamorphic rocks, pre-Early Devonian sedimentary cover and Middle Devonian conglomerate in the Simao-Indochina block lithologically resemble those of the Yangtze block, suggesting a Cambrian–Silurian linkage between these two blocks (YunnanBGMR 1990; Zhong 1998). Existence of Silurian continental rifting-related amphibolite xenoliths (439–404 Ma) in the Jinshajiang ophiolitic rocks indicates that the Yangtze-Indochina initial breakup may be traced to Early Silurian (Jian et al. 2009). Following the breakup of the Simao-Indochina block from the Yangtze block, the Paleotethyan branch ocean and subsequent oceanic subduction developed (Metcalfe 1996; Fan et al. 2010; Lai et al. 2014a; Zhang et al. 2014a) along the JAS suture.

The Jinshajiang–Ailaoshan–Song Ma Ocean may have commenced its closure by subducting westward beneath

Fig. 3 Outcrop photos (**a**, **c**) and micrographs (**b**, **d**) for the Mengdong amphibolites (YN-24) and Wana granitic gneisses (HH-122). The features are hornblende (Hbl), quartz (Qz), plagioclase (Pl), pyroxene (Pyr) and biotite (Bt)

the Simao-Indochina block during Late Carboniferous (Kamvong et al. 2014; Zi et al. 2012b). Westwards subduction beneath Indochina is proposed because three magmatic phases were identified in southwest of the JAS suture involving the Late Carboniferous–earliest Middle Permian incipient back-arc rift magmatism (Fan et al. 2010; Jian et al. 2009; Zi et al. 2012a, b), Middle Permian arc/back-arc basin magmatism (Fan et al. 2010; Liu et al. 2012; Zi et al. 2012a) and Late Permian to earliest Triassic arc magmatism (Lai et al. 2014b; Liu et al. 2015; Zi et al. 2012a). Convergent margin magmatism which is represented by the 252 Ma Xin'anzhai (Liu et al. 2015) and Baimaxueshan plutons (Zi et al. 2012a) and 248 Ma Maoheshan basalts (Liu et al. 2012) terminated at around 247 Ma (Liu et al. 2015). Termination of convergent plate activity was immediately followed by regional compressive deformation and high-grade metamorphism. The compression regime marks the commencement of the Indosinian Orogeny associated with assembly of the Yangtze and Simao-Indochina blocks (Liu et al. 2015).

Along the Ailaoshan tectonic zone, there occurred the well-studied Ailaoshan metamorphic domain (Lin et al. 2012; Zhong 1998), which consists of amphibolite to granulite facies rocks including paragneiss, amphibolite, granitic gneiss, hornblende-schist and marble. Our Wana samples (HH-122 and DX-12) were collected from this metamorphic domain. The samples are granitic gneisses and contain 45–55 vol% quartz, 25–35 vol% plagioclase, 5–10 vol% biotite and minor amount of magnetite, zircon and apatite (Fig. 3). To southeast of the Ailaoshan metamorphic domain, there occurred the Dulong-Song Chay granitic batholith with the crystallization age of ~430 Ma (Peng et al. 2015). The protolith gabbro of the Mengdong amphibolite intruded into the Dulong-Song Chay batholith (Fig. 3a), and the amphibolite samples exhibit medium- to coarse-grained meta-igneous textures, which contain 50–60 vol% hornblende, 15–20 vol% plagioclase, ~5 vol% pyroxene, ~5 vol% quartz, ~2 vol% biotite and small amounts of chlorite, epidote, magnetite, zircon and apatite.

Analytical methods

Zircon mineral separates were prepared by conventional heavy liquid and magnetic techniques. Grains were

mounted in epoxy, polished and coated with gold. Their internal texture was examined using cathodoluminescence (CL) imaging at the Institute of Geology and Geophysics (IGG), Chinese Academy of Sciences (CAS), Beijing.

Zircon U–Pb ages and trace elements for samples HH-122A and DX-12C were analyzed using a Laser ICP-MS at the IGG CAS. The zircon standards CN92-2, 91500 and GJ-1 were used to calibrate the U–Th–Pb ratios. The spot size for data collection was 30 μm. The errors for individual U–Pb analyses are presented with 1σ error, and uncertainties in grouped ages are quoted at 95 % level (2σ). The age calculations and plots were made using Isoplot (version 3.0; Ludwig 2001). Further detailed descriptions of the instrumentation and analytical procedure for the LA-ICP-MS zircon U–Pb and trace element technique are similar to those described by Yuan et al. (2004).

Measurements of U, Th and Pb for sample YN-24A were taken using the Cameca IMS-1280 at IGG CAS. U–Th–Pb ratios were determined relative to the standard zircon Plesˇovice, and their absolute abundances were calibrated to the standard zircon 91500 (Wiedenbeck et al. 1995), using operating and data processing procedures similar to those described by (Li et al. 2009). Any effects from surface contamination were minimized by pre-rastering a ~20-mm surface area for 180 s prior to analysis. Standard analyses were carried out after every three unknown analyses. Calculated Th/U ratios in all unknown samples were obtained by comparison with measured Th/U ratios (Th/U = 0362) and $^{206}Pb/^{238}U$ in zircon standard 91500 assuming closed-system behavior. A long-term uncertainty of 1.5 % (1 RSD—relative standard deviation) for $^{206}Pb/^{238}U$ measurements of the standard zircons was propagated to the unknowns (Li et al. 2009), despite the fact that the measured $^{206}Pb/^{238}U$ error in a specific session was generally around 1 % (1 RSD) or less. Measured compositions were corrected for common Pb using ^{204}Pb correction. The weighted mean U–Pb ages and Concordia plots were processed using Isoplot/Ex version 3.0 program (Ludwig 2001). SIMS zircon U–Pb isotopic data are presented in Supplemental table 1.

Zircon Lu–Hf isotopic analysis was carried out using a Geolas-193 laser ablation microprobe, attached to a Neptune multi-collector ICP-MS at the IGG CAS. All of the settings yielded a signal intensity of ~10 Vat ^{180}Hf for the standard zircon 91500 with a recommended $^{176}Hf/^{177}Hf$ ratio of 0.282293 ± 28 (Wu et al. 2006). Data were normalized to $^{176}Hf/^{177}Hf = 0.7325$, using exponential correction for mass bias. The mean βYb value was applied for the isobaric interference correction of ^{176}Yb on ^{176}Hf in the same spot. The ratio of $^{176}Yb/^{172}Yb$ (0.5887) was also applied for the Yb correction.

Whole-rock samples for geochemistry were crushed to 200-mesh using an agate mill for elemental and Sr–Nd isotopic analyses. The major oxides were analyzed by a wavelength X-ray fluorescence spectrometry at the State Key Laboratory of Isotope Geochemistry, Guangzhou Institute of Geochemistry (GIG), Chinese Academy of Sciences (CAS). Trace element analyses were performed at the GIG CAS by a Perkin-Elmer Sciex ELAN 6000 ICP-MS. Detailed sample preparation and analytical procedure followed Li et al. (2002). Sr, Nd isotopic analyses were carried out at the GIG CAS on a Neptune Plus (Thermo Fisher Scientific, MA, USA) multi-collection mass spectrometry equipped with nine Faraday cup collectors and eight ion counters. Details analytical methods are presented by (Yang et al. 2006). Normalizing factors used to correct the mass fractionation of Sr and Nd during the measurements were $^{86}Sr/^{88}Sr = 0.1194$ and $^{146}Nd/^{144}Nd = 0.7219$ (Yang et al. 2007).

Analytical results

Least altered metagabbro and granitic gneiss samples were taken from the Mengdong and Wana villages, respectively, for zircon U–Pb geochronological, in situ Lu–Hf isotopic, whole-rock elemental and Sr–Nd isotopic analyses. The analytical results are listed in Supplemental tables 1–4.

Zircon U–Pb geochronology and in situ Lu–Hf isotopes

In order to determinate the absolute age, granitic gneiss samples DX-12C and HH-122A were selected for LA-ICPMS zircon U–Pb dating and amphibolite sample YN-24A for SIMS zircon U–Pb dating. Zircon grains from sample DX-12C are prismatic, euhedral and 100–200 μm by 50–120 μm in size without inherited cores. Zircon grains from sample HH-122A have oscillatory zoning with inherited cores and are mostly euhedral, transparent to colorless with the lengths of 80–200 μm and widths of 50–100 μm (Fig. 4). Zircon crystals from sample YN-24A are uniform with large gray luminescent cores and pale rims. Dating results are listed in Supplemental tables 1–2 and presented on concordia plots in Fig. 4. Lu–Hf isotopic results for the dated samples are listed in Supplemental table 3 and shown in Fig. 5. Initial Hf isotopic ratios are recalculated to the crystallization ages, using the ^{176}Lu–^{176}Hf decay constant reported by Soderlund et al. (2004). $^{176}Lu/^{177}Hf$ ratios of most zircons are <0.003, indicating a low radiogenic growth of ^{176}Hf. Two-stage model ages (T_{DM2}) are calculated for the source rocks by assuming a mean $^{176}Lu/^{177}Hf$ value of 0.015 for the average continental crust (Griffin et al. 2002).

Twenty SIMS geochronological analyses were performed on 20 zircons from sample YN-24A and give high and variable Th/U ratios of 0.01 to 5.9 (most of them >0.1).

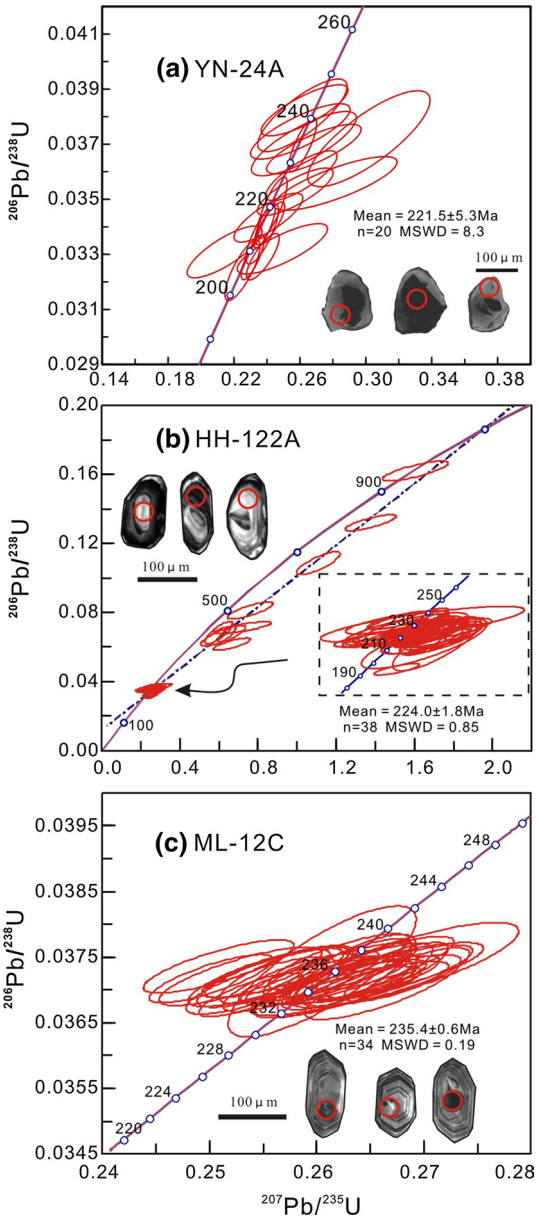

Fig. 4 SIMS zircon U–Pb concordia diagrams for the Mengdong amphibolites (**a**) and LA-ICP-MS zircon U–Pb concordia diagrams for the Wana granitic gneisses (**b**, **c**). *Red circles* on CL images mark analytical site on each grain

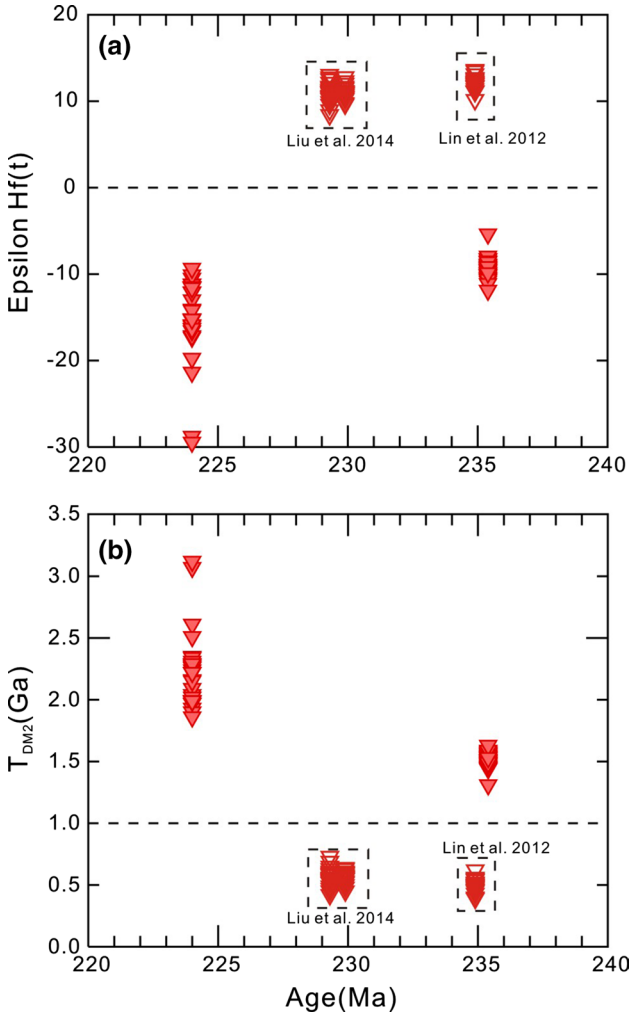

Fig. 5 Zircon ages (Ma) versus $\varepsilon_{Hf}(t)$ (**a**) and T_{DM2}(Hf) (**b**) for zircons from the Wana granitic gneisses along the Ailaoshan suture

Metamorphic zircons always show lower Th/U ratios and younger isotopic ages than their primary magmatic zircons. However, the two spots with lowest Th/U ratios (YN-24A-11 and YN-24A-13) have $^{206}Pb/^{238}U$ apparent ages of 217.6 Ma and 240.7 Ma, and the two spots with highest Th/U ratios (YN-24A-1 and YN-24A-5) have $^{206}Pb/^{238}U$ apparent ages of 208.6 Ma and 241.7 Ma. These characteristics suggest that the U–Pb isotopic systems of our analyzed zircons have not been disturbed by the amphibolite facies metamorphism. The protolith gabbro of the Mengdong amphibolite intruded into the Dulong-Song Chay batholith (~430 Ma), but no early Paleozoic or older zircon ages have been detected in the sample YN-24, indicating the absence of inheritance. Our 20 spots yield $^{206}Pb/^{238}U$ apparent ages of 205.7–241.9 Ma and a weighted mean $^{206}Pb/^{238}U$ age of 221.5 ± 5.3 Ma (MSWD = 8.3, Fig. 4a), which was interpreted as the crystallization age of the protolith gabbro.

Forty-eight analyses were performed on 48 zircon grains from sample HH-122A and document Th/U ratios ranging from 0.10 to 0.68 with two exceptions, consistent with an igneous origin (Wu and Zheng 2004). Except ten analyses showing inherited $^{206}Pb/^{238}U$ ages, the remaining 38 analyses yield $^{206}Pb/^{238}U$ apparent ages of 215.1–236.9 Ma and a weighted mean age of 224.0 ± 1.8 Ma (n = 38, MSWD = 0.85; Fig. 4b). The grains with the Indosinian crystallization age (224.0 ± 1.8 Ma) show negative $\varepsilon_{Hf}(t)$ values (−29.5 to −9.4, Fig. 5a) and old T_{DM2} ages (1.86–3.12 Ga, Fig. 5b).

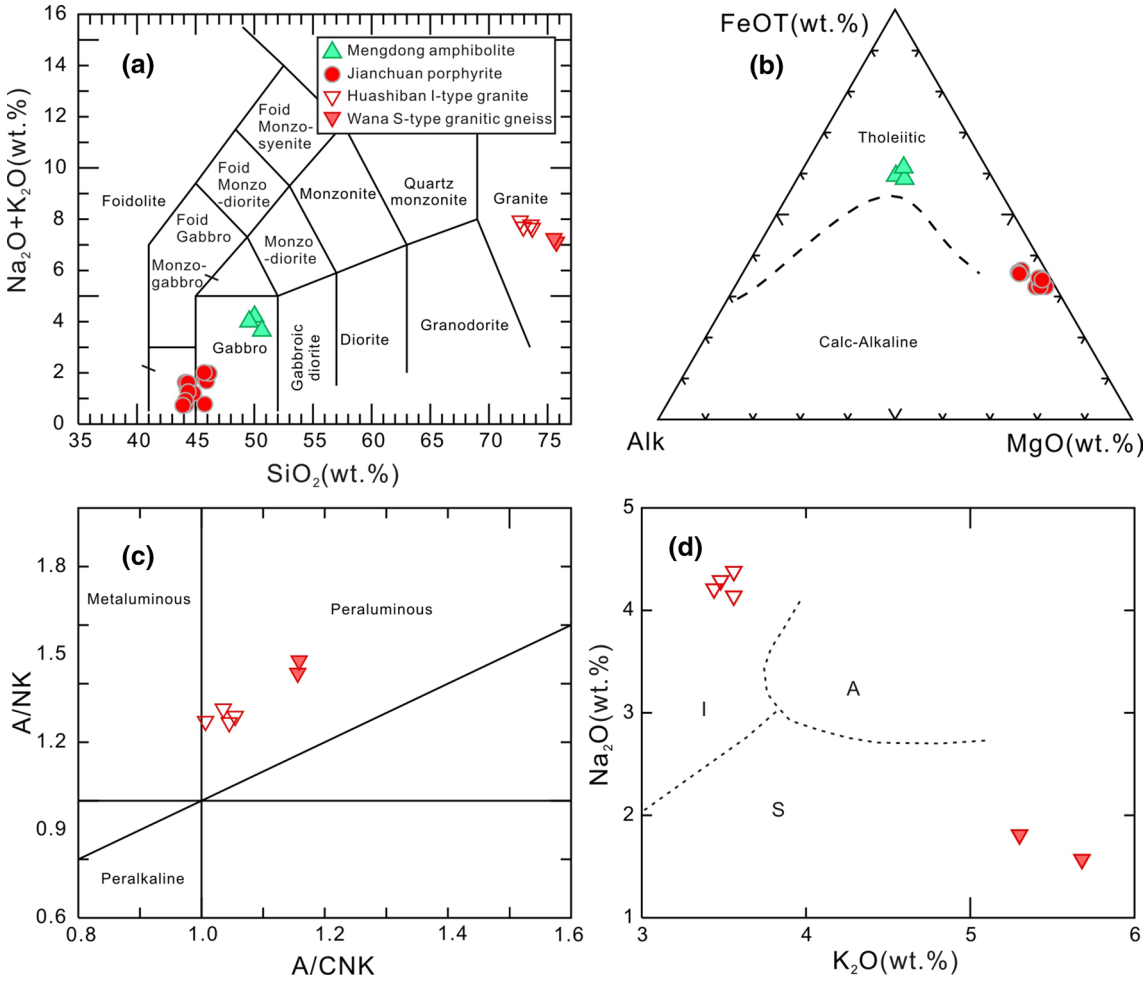

Fig. 6 **a** SiO_2–K_2O + Na_2O plot (Le Bas et al. 1986); **b** AFM plot (Irvine and Baragar 1971); **c** A/NK versus A/CNK plot; **d** K_2O versus Na_2O plot

Thirty-five analyses were performed on 35 zircons from sample DX-12C. Except one Ordovician zircon (495.6 Ma), they yield very concordant $^{206}Pb/^{238}U$ apparent ages ranging from 233.7 to 236.9 Ma, with a weighted mean $^{206}Pb/^{238}U$ age of 235.4 ± 0.6 Ma (n = 34, MSWD = 0.19, Fig. 4c). Except one spot with Th/U < 0.1, the remaining 33 spots have Th/U ratios varying from 0.30 to 1.08, consistent with an igneous origin (Wu and Zheng 2004). $\varepsilon_{Hf}(t)$ values for the 34 grains with the crystallization age range from −11.9 to −5.4 (Fig. 5a) and T_{DM2} ages from 1.61 Ga to 2.02 Ga.

Whole-rock geochemical results

The whole-rock major oxides, trace elemental and Sr–Nd isotopic data for the studied samples are listed in Supplemental table 2. The Mengdong samples plot into the gabbro field on the TAS diagram (Fig. 6a) and define a typical tholeiite compositional trend on the AFM diagram (Fig. 6b). The Mengdong amphibolites have low $Mg^{\#}$ (41.7–42.8), high TiO_2 (~3.7 wt%) and Na_2O (Na_2O/K_2O = 1.89–2.68) contents. They exhibit similar chondrite-normalized REE patterns with the OIB (Fig. 7b), with strongly enriched LREE contents and insignificant Eu anomalies (Eu* = 0.99–1.03). Their primitive mantle-normalized element spidergrams show moderate negative Sr anomalies (Sr* = 0.46–0.56; Fig. 7a). Such geochemical signatures are comparable to those of OIB, but markedly distinct from those of E-MORB, N-MORB (Sun and McDonough 1989) and arc volcanics. The Mengdong samples have $(^{87}Sr/^{86}Sr)i$ ratios of 0.707647 and $\varepsilon_{Nd}(t)$ values of +1.17 (Fig. 8).

The Wana granitic gneisses (HH-122A and 122B) exhibit high A/CNK values (>1.1; Fig. 6c) low FeOt, Na_2O, TiO_2 and P_2O_5 but high K_2O contents (K_2O/Na_2O = 2.93–3.63; Fig. 6d). CIPW-normalized corundum contents range from 1.89 to 2.02, more than 1.0 vol%. These signatures are consistent with those of the S-type granites (Clemens

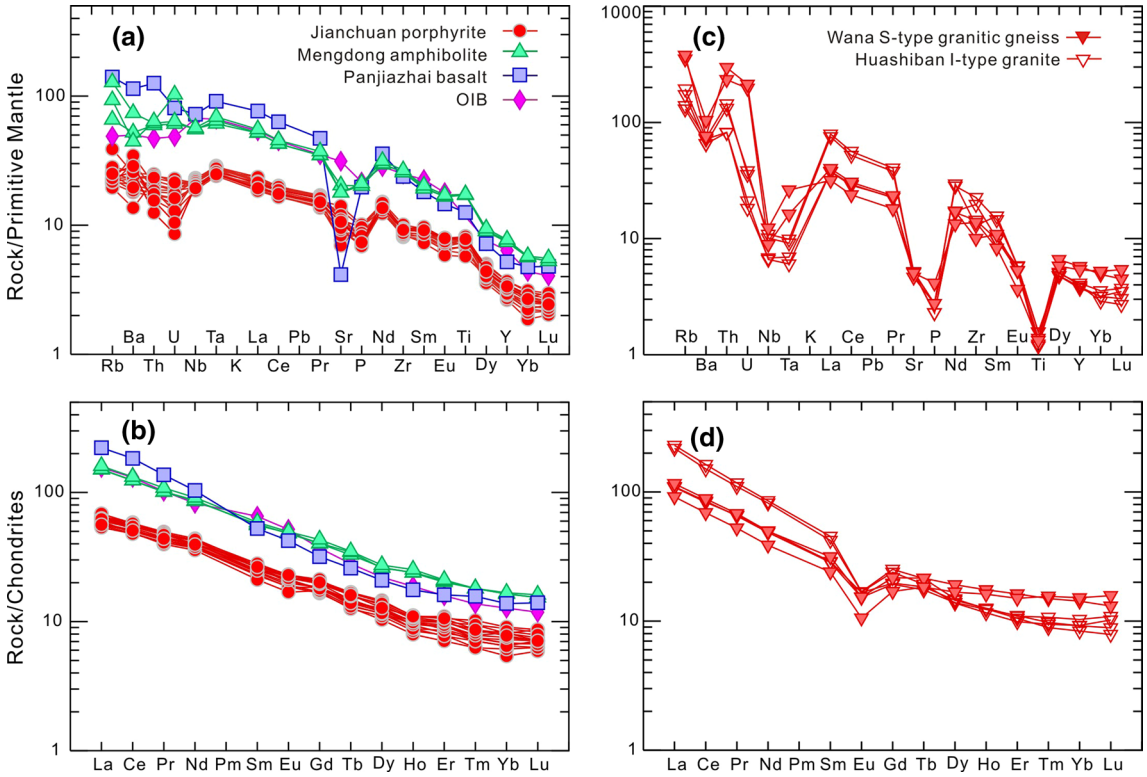

Fig. 7 Primitive mantle-normalized incompatible elemental spidergrams and chondrite-normalized REE patterns for the Mengdong amphibolites (**a**, **b**) and Wana granitic gneisses (**c**, **d**). Normalized values for primitive mantle and chondrite are from Sun and McDonough (1989)

2003). The Wana granitic gneisses show LREE-enriched chondrite-normalized REE patterns with significant Eu anomalies (Fig. 7d). On the primitive mantle-normalized spider diagram (Fig. 7c), they are characterized by strong depletions in Ba, Nb, Ta, Sr and Ti and enrichment in Th, U and K. The initial Sr isotopic ratios for the Wana granitic gneisses vary from 0.718589 to 0.719754, and $\varepsilon_{Nd}(t)$ values range from −11.34 to −10.92 (Fig. 8).

Discussion

Petrogenesis of the OIB-like amphibolites

The Mengdong amphibolites are newly exposed due to the road mending (Fig. 3a), and the amphibolite samples are fresh with low LOI values (0.41–0.57 wt%). Our samples show smooth and coherent chondrite-normalized REE and primitive mantle-normalized trace element diagrams without Th, Nb and Rb anomalies (Fig. 7), suggesting that the incompatible elements in the amphibolite samples have not been affected significantly by the post-magmatism metamorphism. The lithophile isotopic systems, such as Rb–Sr, Sm–Nd and U–Pb, are both incompatible and will not get fractionated, and thus post-magmatism metamorphism has not altered the isotopic compositions. The geochemical characteristics of the Mengdong amphibolites were more likely controlled by the source nature and petrogenetic processes of the protolith gabbros. In general, depleted mantle-derived primary melts have Ni > 400 ppm and Cr > 1000 ppm, and $Mg^{\#}$ = 73–81 (Litvak and Poma 2010), and enriched mantle-derived primary melts have $Mg^{\#}$ > 65 (Kamenetsky et al. 2003). The low $Mg^{\#}$ and compatible element contents such as Cr (33.8–38.5 ppm) and Ni (40.3–45.3 ppm) for the Mengdong amphibolites indicate significant fractionation of olivine and clinopyroxene during magma evolution of the protolith gabbros. Because Sr is compatible in plagioclase, moderate negative Sr anomalies in comparison with the typical OIB may suggest the importance of plagioclase in the fractional crystallization (Sun and McDonough 1989). The lack of a negative Eu anomaly in the evolved lava is common for the OIB-like mafic rocks (Xu et al. 2001) and may reflect a high Eu^{3+}/Eu^{2+} ratio in magma (Frey et al. 1993).

In the western margin of the Yangtze block, the OIB-like mafic rocks were considered to originate from partial melting of an incipient OIB-type mantle source, and three distinct additional petrogenic processes have been invoked to account for their elemental diversity: (1) contamination of upper crust; (2) contamination of subcontinental

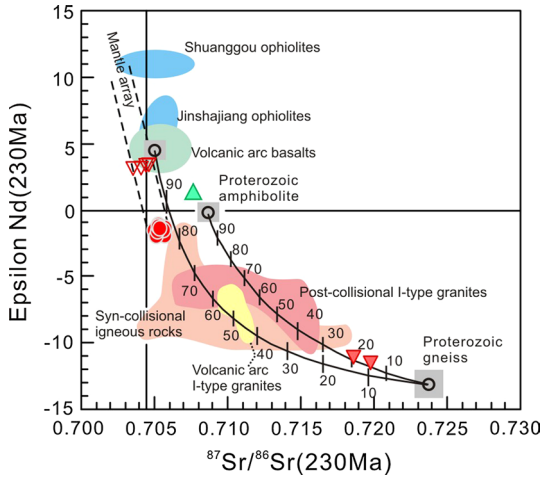

Fig. 8 $^{87}Sr/^{86}Sr$ (t) versus $\varepsilon_{Nd}(t)$ diagram. Data for the Shuanggou and Jinshajiang ophiolites are from Xu and Castillo (2004). Data for the volcanic arc basalts are from (Fan et al. 2010). The fields of the volcanic arc I-type granites, syn-collisional igneous rocks and post-collisional I-type granites are from Zi et al. (2012a, c) and Zhu et al. (2011), respectively. The number marked on the mixing curves notes mass fractions (%) of the mafic component in the mixed source. Sr (ppm), Nd (ppm), $(^{87}Sr/^{86}Sr)i$ and $\varepsilon_{Nd}(t)$ for the end members used in mixing calculation are 229.4, 23.6, 0.708581 and −0.27 for the Proterozoic amphibolite (Cai et al. 2014), 141.9, 33.2, 0.723649 and −13.17 for the Proterozoic gneiss (Wang et al. under review) and 350.0, 13.0, 0.704988 and 4.50 for the volcanic arc basalts (Fan et al. 2010), respectively. Symbols are the same as in Fig. 6

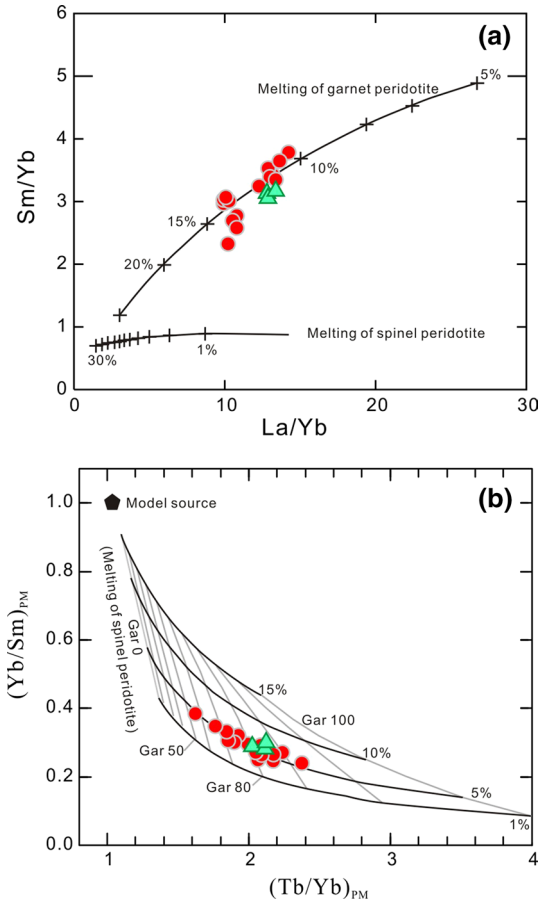

Fig. 9 **a** $(Tb/Yb)_{PM}$ versus $(Yb/Sm)_{PM}$ (after Zhang et al. 2006). The *grid* indicates the range of model compositions. The proportion of melt formed in the presence of garnet is indicated by *light lines*; curves of constant melt fraction are shown with *heavy lines*. The data used to model are seen in Zhang et al. (2006) and references therein. **b** Sm/Yb versus La/Yb plot. The batch melting curves are from Zi et al. (2010)

lithospheric mantle (SCLM); (3) input of MORB-like depleted component (Kou et al. 2012; Xu et al. 2001; Zhang et al. 2006; Zi et al. 2010). Crustal contamination to the protolith gabbro of the Mengdong amphibolite was minimal as evidenced from the following observations: (1) the absence of inherited zircons and (2) no notable Nb, Ta and Eu negative anomalies. Thus, contamination of upper crust (model 1) is excluded. The Emeishan low-Ti basalts which contain a notable contribution from the SCLM show low Ti/Y (<500), Nb/La ratios (<1), Fe_2O_3T contents (<12 wt%) and $Mg^{\#}$ of 52–64, in contrast to our Mengdong samples with high Ti/Y (639–671), Nb/La ratios (1.07–1.12), Fe_2O_3T contents (13.85–14.08 wt%) and low $Mg^{\#}$ (41.7–42.8; Xu et al. 2001). Contamination of SCLM is also excluded. The OIB-type mantle may be represented by the Yanyuan gabbros related to the Emeishan plume with high $\varepsilon_{Nd}(t)$ (4.87 to 5.13) and low $(^{87}Sr/^{86}Sr)i$ ratios (0.703752 to 0.703844; Xu et al. 2001), and the MORB-like depleted component may be represented by the gabbros from the Ailaoshan ophiolites with $\varepsilon_{Nd}(t) = +10.3$ to $+11.5$ and $(^{87}Sr/^{86}Sr)i = 0.70356$–$0.70618$ (Xu and Castillo 2004). Both of them show much more depleted Sr–Nd isotopic compositions than the Mengdong amphibolites; thus, their mixing results could not be more enriched than the Mengdong amphibolites. The Mengdong amphibolites are identical to the subtype 1 of the high-Ti lavas (HT1) in the Emeishan flood basalt province, which exhibit high TiO_2 (3.65–4.7 wt%), Fe_2O_3T (12.7–16.4 wt%), Nb/La (0.75–1.1), coupled with higher $\varepsilon_{Nd}(t)$ (1.1–4.8) and lower SiO_2 (45–51 wt%; Xu et al. 2001). The HT1 lavas originated from an OIB-like mantle source and have experienced an AFC style of contamination in the upper crust. However, in comparison with HT1 lavas, the Mengdong amphibolites show invisibly Nb, Ta and Th anomalies and crustal contamination was insignificant as aforementioned. Thus, we prefer a homogeneous OIB-type mantle source without significant contamination or magma mixing for the Mengdong amphibolites.

Incompatible trace element ratios, such as Ce/Y and Zr/Nb, Tb/Yb and Yb/Sm, La/Yb and Sm/Yb, can provide constraints on the nature of the mantle source. A plot of Sm/Yb versus La/Yb (Fig. 9a) enables differentiation

between the melting of spinel and garnet peridotite because the heavy REE Yb is compatible in garnet (Zi et al. 2010), whereas La and Sm are incompatible, such that La/Yb and Sm/Yb will be strongly fractionated when the degree of melting is low. In contrast, La/Yb is only slightly fractionated and Sm/Yb is nearly unfractionated during melting in the spinel stability field (Aldanmaz et al. 2000). Figure 9a shows that low degrees (<15 %) of batch melting of the OIB-type mantle source [$(La/Yb)n > 1$] in the garnet stability field can generate the La/Yb–Sm/Yb systematics of the Mengdong amphibolites. In $(Tb/Yb)_{PM}$ versus $(Yb/Sm)_{PM}$ diagram (Fig. 9b), all the samples lie close to the melt path for garnet peridotite rather than the path for spinel peridotite. Low-degree partial melting of garnet stability mantle source for the Mengdong amphibolites is also supported by the trends shown in La/Sm versus Sm/Yb and Ce/Y versus Zr/Nb diagrams (Supplemental Fig. 1). The presence of garnet indicates melting of the peridotite at considerable depth (>80 km; Xu et al. 2001).

Petrogenesis of the S-type granitoids

The Wana granitic gneisses are strongly peraluminous S-type granites and show low and negative $\varepsilon_{Nd}(t)$ of −11.34 to −10.92 and $\varepsilon_{Hf}(t)$ values of −29.5 to −5.4, and low Na_2O contents (K_2O/Na_2O = 2.93–3.63). Strongly peraluminous granites may originate from (1) aluminum-rich meta-sedimentary rocks (Miller 1985), (2) amphibolites under H_2O-rich conditions (Ellis and Thompson 1986) or (3) fractionation of aluminous-poor magma (Zen 1986). The products from either case (2) or (3) are usually characterized by enrichment of Na and Sr (Ellis and Thompson 1986; Zen 1986), which contrasts to the Wana granitic gneisses. High A/CNK ratios and low and negative $\varepsilon_{Nd}(t)$–$\varepsilon_{Hf}(t)$ values argue against the involvement of a mantle-derived mafic component. This is also in agreement with the presence of the Caledonian and Proterozoic inherited zircons and Proterozoic zircon Hf model ages. In summary, the Wana gneisses are product of dehydration melting of the meta-sedimentary rocks.

Tectonic settings for the OIB-like gabbros and associated rocks

The OIB-like rocks have previously been linked to localized and/or regional extension, which may occur through: (1) mantle plume activity (Buiter and Torsvik 2014; Xu et al. 2001; Zi et al. 2010); (2) lithospheric delamination (Cawood and Williams 1988); (3) slab rollback induced back-arc extension (Nakakuki and Mura 2013); (4) the subducted slab break-off (Caprarelli and Leitch 2001). The Emeishan plume happened in Late Permian (Wang et al. 2012; Xu and Castillo 2004), and thus the Late Triassic Mengdong amphibolites cannot be associated with it. The mantle plume-related mechanism (model 1) is excluded. The lithospheric delamination (model 2) would bring the asthenosphere close to the Moho with a relatively shallow depth of melting of the asthenosphere and related magmatism would be very extensive (Bao et al. 2014). However, the Mengdong and Jianchuan OIB-like magmas were formed at considerable depth (<80 km) and are notably small scale. In western Yangtze block, significant lithospheric delamination happened during the Late Paleogene after the India–Asia continental collision (Lu et al. 2015). Hence, the lithospheric delamination (model 2) is not favored. Slab rollback is often accompanied by the oceanic crust subducting, but the arc magmatism along the Ailaoshan suture zone has terminated in Early Triassic (as aforementioned in "Geological background" section). In addition, the Paleotethys-related arc magmatism was located in southwest of Ailaoshan ophiolites and the Mengdong gabbroic intrusion in northeast. Therefore, the slab rollback model could not generate the Mengdong OIB-like rocks. The slab break-off predicts a linear zone of magmatism (Nakakuki and Mura 2013; Tian et al. 2011), and this is the case for the spatial distribution of the Late Triassic igneous rocks along the South China-Indochina suture zone. We prefer the slab break-off model for petrogenesis of the Mengdong amphibolites.

Experimental data have demonstrated that biotite, muscovite and feldspar in paragneiss will breakdown when the temperature is higher than 800–850 °C (Thompson and Connolly 1995), but dehydration melting of amphibolites requires much higher temperatures (>1000 °C, Rapp and Watson 1995). The continental arc, syn-collisional and post-collisional settings could provide sufficient thermal budget to induce the partial melting of the meta-sedimentary rocks; thus, the Wana S-type granitic gneisses may be generated in various tectonic settings. However, in the Ailaoshan suture zone, another type of Late Triassic granitoids should be mentioned, the high $\varepsilon_{Nd}(t)$–$\varepsilon_{Hf}(t)$ I-type Huashiban granodiorites (Liu et al. 2014). They are high-K calc-alkaline I-type granites which are derived from the partial melting of a juvenile mafic crust. The thermal budget provided by radioactive decay and crustal thickening would be insufficient to trigger the partial melting of the mafic source at lower crust levels without additional heat input from the mantle processes. In consideration of the heat source, the high-K calc-alkaline I-type granites only occurred in two tectonic scenarios: (1) continental arc settings similar to that of the Andes and (2) post-collisional extensions similar to that of the Caledonia (Roberts and Clemens 1993). As aforementioned, the arc magmatism along the Ailaoshan suture zone terminated in Early Triassic. We prefer a post-collisional setting for the Late Triassic S- and I-type granitoids along the South China and Indochina suture zone.

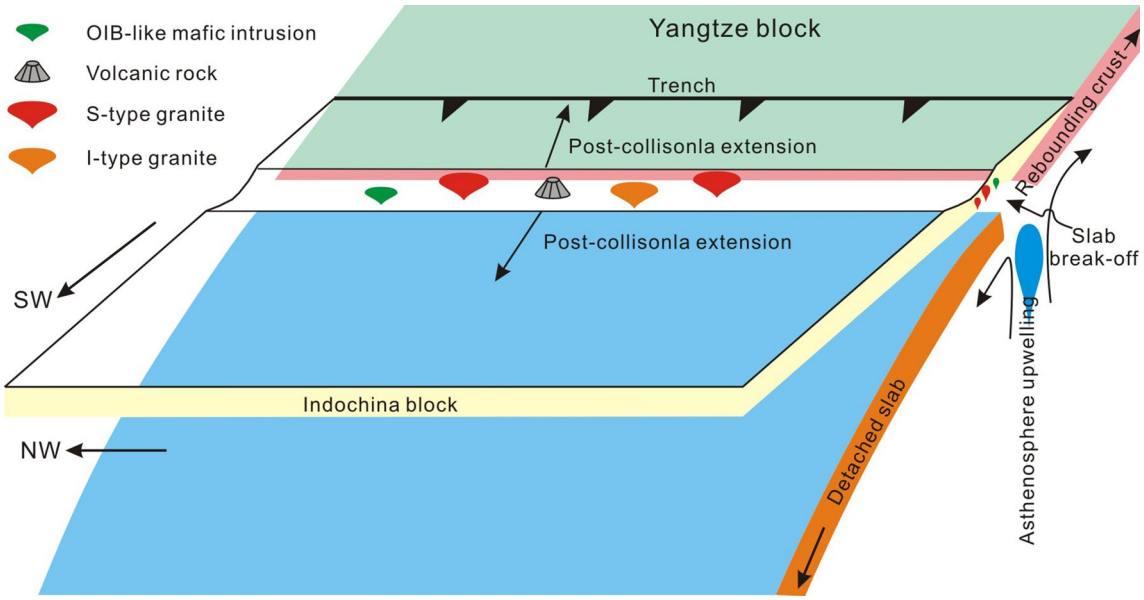

Fig. 10 Schematic cartoon illustrating the slab break-off and asthenosphere upwelling processes, and generation of OIB-like mafic rocks, S-type and I-type granites

In summary, we proposed a post-collisional slab break-off model for the petrogenesis of the Mengdong amphibolites, Wana S-type and Huashiban I-type granitoids (Fig. 10).

Implications for the Indosinian Orogeny

After the termination of the arc magmatism (~250 Ma; Supplemental table 5), the collision of continental blocks along the JAS suture has been recorded by syn-collisional felsic rocks (Supplemental table 5) and syn-kinematic metamorphism (e.g., Liu et al. 2015; Zhang et al. 2011). The Tongtiange leucogranites (~247 Ma), Phia Bioc granites (248–245 Ma) and high-Si rhyolites (247–246 Ma) in the Gaoshanzhai, Pantiange and Renzhixueshan formations are related to syn-collisional crust thickening (Liu et al. 2011; Zi et al. 2012c; Roger et al. 2012). The syn-kinematic hornblende, biotite and muscovite formed in a series of northwest to west–northwest trending dextral strike-slip and transpression shear zones along the JAS suture yielded $^{40}Ar/^{39}Ar$ plateau ages ranging from 250 to 240 Ma (Lepvrier et al. 1997, 2004; Maluski et al. 2005). Metamorphic zircons and monazites in high-grade rocks in northern Vietnam give similar ages of 250–243 Ma (Carter et al. 2001; Nam et al. 1998; Roger et al. 2003, 2007; Nakano et al. 2010). In addition, the pre-Permian strata were overlain unconformably by the Gaoshanzhai and Pantiange Formations and their along-strike equivalents mainly composed of coarse-grained sedimentary rocks, indicating a terrestrial depositional environment (YunnanBGMR 1990; Zhong 1998). These lines of evidence suggest that the initial collision of the Simao (Indochina) and Yangtze blocks probably took place in the Early Triassic (~247 Ma).

Following the Early Triassic syn-collisional magmatism and metamorphism, Late Triassic (235–224 Ma) OIB-like mafic and S-type felsic rocks were identified in this study. Late Triassic granitoids are widespread along the JAS suture zone, e.g., the Ludian granodiorite–monzogranite [214–231 Ma, (Zi et al. 2013)], the Yangla and Gongka granodiorite [230–232 Ma, (Gao et al. 2010)], the Beiwu granodiorite [234 Ma, (Zhu et al. 2011)], the Linong monzogranite [233 Ma, (Zhu et al. 2011)] and the Lunong granodiorite [231 Ma, (Zhu et al. 2011)] in the Jinshajiang area, the granodioritic mylonite (233 Ma) in Diancangshan area (Li et al. 2008), the Kontum Grt granite [233 Ma; (Owada et al. 2006)], the Dien bien granodiorite [232–226 Ma; (Roger et al. 2014)], the Truong son granodiorite and monzonite [229–202 Ma; (Liu et al. 2012)], the Chieng Khuong granite [222 Ma; (Zhang et al. 2014b)] in the Song Ma area. These rocks have been interpreted as a result of remelting of the ancient continental crust. Besides, the high $\varepsilon_{Nd}(t)$–$\varepsilon_{Hf}(t)$ Huashiban (~229 Ma) and Xiaguan granodiorites (234 Ma) were originated from juvenile basic continental crust (Liu et al. 2014).

How to interpret this Late Triassic magmatic "flare-up" is still a pending problem. Herein we should mention the sporadically cropping out Late Triassic high- or ultrahigh-pressure metamorphic rocks, e.g., the pelitic granulites in Diancangshan area (Qi et al. 2012), the mafic granulites (Nakano et al. 2008; Zhang et al. 2014b), eclogites (231 Ma) and garnet hornblende rock (228 Ma; Zhang et al.

2013, 2014b) in northern Vietnam. Slab break-off has been suggested to occur usually following the continental collision (Atherton and Ghani 2002; Davies and Von Blanckenburg 1995; Gulmez et al. 2013). In continental collision settings, the continuous subduction results in the high-pressure (HP) to ultrahigh-pressure (UHP) metamorphism of the subducting slab and continental crust to form eclogite and granulite, respectively. The eclogitized slab gets denser and will continue to sink, whereas the buoyant continental lithosphere will tend to float to the surface. The rebounding continental crust will carry the UP–UHP metamorphic rocks to the surface, and the upwelling asthenospheric mantle supplies enough heat to induce partial melting of the enriched lithospheric mantle, and overlying lower and upper crust, producing magmatism with within-plate geochemical features. The Late Triassic magmatic "flare-up," including mantle-derived OIB-like mafic rocks, S-type and I-type granites, was generated in post-collisional slab break-off setting (Fig. 10).

Evidence in favor of a slab break-off model for the JAS suture also includes: (1) the observation that, by the late Middle Triassic, the Simao terrane served as a foreland basin characterized by back-thrusting or migration of the orogenic belt toward the terrane (YunnanBGMR 1990). This back-thrust movement might have been initiated by rebound of partially subducted continental lithosphere in response to slab break-off, which may also have been responsible for the exhumation of the metamorphic core complexes (e.g., those exposed along the Diancangshan–Ailaoshan belt). (2) Coal-bearing formations were deposited in clastic rocks that accumulated within JASS (Wang et al. 2014), and a regional angular unconformity separates the coal-bearing formations (e.g., the Hongpo, Dongdu, Shizhongshan and Waigucun Formations) from the underlying strata and ophiolitic mélange (YunnanBGMR 1990). (3) Shen et al. (1998) identified a suite of continental rift volcanic rocks around the Panjiazhai village (Fig. 7).

Conclusions

We draw the following major conclusions based on our new geochronological and geochemical data:

1. The Mengdong amphibolites (222 Ma) show OIB-like geochemical characteristics and were derived from low-degree partial melting of a homogeneous OIB-type mantle source in the garnet stability field.
2. The Wana granitic gneisses are strongly peraluminous S-type granitoids and product of the dehydration melting of meta-sedimentary rocks.
3. A significant Late Triassic magmatic flare-up was recognized along the South China-Indochina suture zone. During the Late Triassic, the South China-Indochina suture zone had transformed into post-collisional setting, and accompanied slab break-off triggered the OIB-type asthenospheric mantle upwelling and provided the heat source for the Late Triassic magmatic flare-up.

Acknowledgments We would like to express our gratitude to Dr. T.-P. Peng and X.-P. Xia for their help during fieldwork, geochemical and zircon U–Pb analyses. Financial supports from National Science Foundation of China (41190073, 41030352), National Basic Research Program of China (2014CB440901), China Postdoctoral Science Foundation (41090280) and "the Fundamental Research Funds for the Central Universities to SYSU" are gratefully acknowledged.

References

Aldanmaz E, Pearce JA, Thirlwall MF, Mitchell JG (2000) Petrogenetic evolution of late Cenozoic, post-collision volcanism in western Anatolia, Turkey. J Volcanol Geotherm Res 102(1–2):67–95

Atherton MP, Ghani AA (2002) Slab breakoff: a model for Caledonian, Late Granite syn-collisional magmatism in the orthotectonic (metamorphic) zone of Scotland and Donegal, Ireland. Lithos 62(3–4):65–85

Bao XW, Eaton DW, Guest B (2014) Plateau uplift in western Canada caused by lithospheric delamination along a craton edge. Nat Geosci 7(11):830–833

Buiter SJH, Torsvik TH (2014) A review of Wilson Cycle plate margins: a role for mantle plumes in continental break-up along sutures? Gondwana Res 26(2):627–653

Cai JX, Zhang KJ (2009) A new model for the Indochina and South China collision during the Late Permian to the Middle Triassic. Tectonophysics 467(1–4):35–43

Cai YF, Wang YJ, Cawood PA, Fan WM, Liu HC, Xing XW, Zhang YZ (2014) Neoproterozoic subduction along the Ailaoshan zone, South China: geochronological and geochemical evidence from amphibolite. Precambrian Res 245:13–28

Caprarelli G, Leitch EC (2001) Geochemical evidence from Lower Permian volcanic rocks of northeast New South Wales for asthenospheric upwelling following slab breakoff. Aust J Earth Sci 48(1):151–166

Carter A, Roques D, Bristow C, Kinny P (2001) Understanding Mesozoic accretion in Southeast Asia: significance of Triassic thermotectonism (Indosinian orogeny) in Vietnam. Geology 29(3):211–214

Cawood PA, Williams H (1988) Acadian basement thrusting, crustal delamination, and structural styles in and around the Humber Arm Allochthon, western Newfoundland. Geology 16(4):370–373

Chen CH, Hsieh PS, Lee CY, Zhou HW (2011) Two episodes of the Indosinian thermal event on the South China Block: constraints from LA-ICPMS U–Pb zircon and electron microprobe monazite ages of the Darongshan S-type granitic suite. Gondwana Res 19(4):1008–1023

Clemens JD (2003) S-type granitic magmas—petrogenetic issues, models and evidence. Earth-Sci Rev 61(1–2):1–18

Davies JH, Von Blanckenburg F (1995) Slab Breakoff—a model of lithosphere detachment and its test in the magmatism and deformation of collisional orogens. Earth Planet Sci Lett 129(1–4):85–102

Deprat J (1914) Etude des plissements et des zones décrasement de la moyenne et de la basse Rivière Noire. Mèmoire du Service Géologique Indochine 3–4:1–59

Ellis DJ, Thompson AB (1986) Subsolidus and partial melting reactions in the quartz-excess CaO+ MgO+ Al_2O_3+ SiO_2+ H_2O system under water-excess and water-deficient conditions to 10 Kb—some implications for the origin of peraluminous melts from mafic rocks. J Petrol 27(1):91–121

Fan WM, Wang YJ, Zhang AM, Zhang FF, Zhang YZ (2010) Permian arc-back-arc basin development along the Ailaoshan tectonic zone: geochemical, isotopic and geochronological evidence from the Mojiang volcanic rocks, Southwest China. Lithos 119(3–4):553–568

Frey FA, Walker N, Stakes DS, Har SR, Nielsen RL (1993) Geochemical characteristics of basaltic glasses from the AMAR and FAMOUS axial valleys, Mid-Atlantic Ridge (36°–37°N): petrogenetic implications. Earth Planet Sci Lett 115(1–4):117–136

Gao R, Xiao L, He Q, Yuan J, Ni PZ, Du JX (2010) Geochronology, geochemistry and petrogenesis of granites in Weixi-Deqin, West Yunnan. Earth Sci J China Univ Geosci 35(2):186–200 **(in Chinese with English abstract)**

Griffin WL, Wang X, Jackson SE, Pearson NJ, O'Reilly SY, Xu XS, Zhou XM (2002) Zircon chemistry and magma mixing, SE China: in-situ analysis of Hf isotopes, Tonglu and Pingtan igneous complexes. Lithos 61(3–4):237–269

Gulmez F, Genc SC, Keskin M, Tuysuz O (2013) A post-collision slab-breakoff model for the orgin of the Middle Eocene magmatic rocks of the Armutlu–Almacik belt, NW Turkey and its regional implications. Geol Soc Spec Publ 372:107–139

Irvine TN, Baragar WRA (1971) A guide to the chemical classification of the common volcanic rocks. Can J Earth Sci 8(5):523–548

Jian P, Liu DY, Kroner A, Zhang Q, Wang YZ, Sun XM, Zhang W (2009) Devonian to Permian plate tectonic cycle of the Paleo-Tethys Orogen in southwest China (II): insights from zircon ages of ophiolites, arc/back-arc assemblages and within-plate igneous rocks and generation of the Emeishan CFB province. Lithos 113(3–4):767–784

Kamenetsky V, Maas R, Eggins S (2003) Chemical diversity of MORB primary melts: ultra-enriched endmember from the Macquarie Island ophiolite. Geophys Res Abstr 5:1–2

Kamvong T, Zaw K, Meffre S, Maas R, Stein H, Lai CK (2014) Adakites in the Truong Son and Loei fold belts, Thailand and Laos: genesis and implications for geodynamics and metallogeny. Gondwana Res 26(1):165–184

Kou CH, Zhang ZC, Santosh M, Huang H, Hou T, Liao BL, Li HB (2012) Picritic porphyrites generated in a slab-window setting: implications for the transition from Paleo-Tethyan to Neo-Tethyan tectonics. Lithos 155:375–391

Lacassin R, Leloup PH, Trinh PT, Tapponnier P (1998) Unconformity of red sandstones in North Vietnam: field evidence for Indosinian orogeny in northern Indochina? Terra Nova 10(2):106–111

Lai CK, Meffre S, Crawford AJ, Zaw K, Halpin JA, Xue CD, Salam A (2014a) The Central Ailaoshan ophiolite and modern analogs. Gondwana Res 26(1):75–88

Lai CK, Meffre S, Crawford AJ, Zaw K, Xue CD, Halpin JA (2014b) The western Ailaoshan Volcanic Belts and their SE Asia connection: a new tectonic model for the Eastern Indochina Block. Gondwana Res 26(1):52–74

Le Bas MJ, Le Maitre RW, Streckeisen A, Zanettin B (1986) A chemical classification of volcanic rocks based on the total alkali-silica diagram. J Petrol 27:745–750

Lepvrier C, Maluski H, Van Vuong N, Rogues D, Axente V, Rangin C (1997) Indosinian NW-trending shear zones within the Truong Son belt (Vietnam) Ar-40–Ar-39 Triassic ages and Cretaceous to Cenozoic overprints. Tectonophysics 283(1–4):105–127

Lepvrier C, Maluski H, Van Tich V, Leyreloup A, Thi PT, Van Vuong N (2004) The Early Triassic Indosinian orogeny in Vietnam (Truong Son Belt and Kontum Massif); implications for the geodynamic evolution of Indochina. Tectonophysics 393(1–4):87–118

Lepvrier C, Van VN, Maluski H, Thi PT, Van VT (2008) Indosinian tectonics in Vietnam. Comptes Rendus Geosci 340(2–3):94–111

Levin V, Shapiro N, Park J, Ritzwoller M (2002) Seismic evidence for catastrophic slab loss beneath Kamchatka. Nature 418(6899):763–767

Li XH, Li ZX, Zhou HW, Liu Y, Kinny PD (2002) U–Pb zircon geochronology, geochemistry and Nd isotopic study of Neoproterozoic bimodal volcanic rocks in the Kangdian Rift of South China: implications for the initial rifting of Rodinia. Precambrian Res 113(1–2):135–154

Li B, Ji J, Fu X, Gong J, Song B, Qing J, Zhang C (2008) Zircon SHRIMP dating and its geological implications of the metamorphic rocks in Ailao Shan-Diancang Mountain Ranges, west Yunnan. Acta Petrol Sin 24(10):2322–2330 **(in Chinese with English abstract)**

Li XH, Liu Y, Li QL, Guo CH, Chamberlain KR (2009) Precise determination of Phanerozoic zircon Pb/Pb age by multicollector SIMS without external standardization. Geochem Geophys Geosyst 10:Q04010. doi:10.1029/2009GC002400

Lin TH, Chung SL, Chiu HY, Wu FY, Yeh MW, Searle MP, Iizuka Y (2012) Zircon U–Pb and Hf isotope constraints from the Ailao Shan-Red River shear zone on the tectonic and crustal evolution of southwestern China. Chem Geol 291(2012):23–37

Litvak VD, Poma S (2010) Geochemistry of mafic Paleocene volcanic rocks in the Valle del Cura region: implications for the petrogenesis of primary mantle-derived melts over the Pampean flat-slab. J S Am Earth Sci 29(3):705–716

Liu C, Deng JF, Liu JL, Shi YL (2011) Characteristics of volcanic rocks from Late Permian to Early Traissic in Ailaoshan tectonomagmatic belt and implications for tectonic settings. Acta Petrol Sin 27(12):3590–3602 **(in Chinese with English abstract)**

Liu JL, Tran MD, Tang Y, Nguyen QL, Tran TH, Wu WB, Chen JF, Zhang ZC, Zhao ZD (2012) Permo-Triassic granitoids in the northern part of the Truong Son belt, NW Vietnam: geochronology, geochemistry and tectonic implications. Gondwana Res 22(2):628–644

Liu HC, Wang YJ, Fan WM, Zi JW, Cai YF, Yang GL (2014) Petrogenesis and tectonic implications of Late-Triassic high E > (Nd)(t)-E > (Hf)(t) granites in the Ailaoshan tectonic zone (SW China). Sci China Earth Sci 57(9):2181–2194

Liu HC, Wang YJ, Cawood PA, Fan WM, Cai YF, Xing XW (2015) Record of Tethyan ocean closure and Indosinian collision along the Ailaoshan suture zone (SW China). Gondwana Res 27(3):1292–1306

Lu YJ, Mccuaig TC, Li ZX, Jourdan F, Hart CJR, Hou ZQ, Tang SH (2015) Paleogene post-collisional lamprophyres in western Yunnan, western Yangtze Craton: mantle source and tectonic implications. Lithos 233:139–161. doi:10.1016/j.lithos.2015.02.003

Ludwig KR (2001) Sqiud 1.02: a user manual. Berkeley Geochronological Center Special Publication, Berkeley, pp 1–219

Maluski H, Lepvrier C, Leyreloupa A, Van TV, Thi PT (2005) Ar-40–Ar-39 geochronology of the charnockites and granulites of the Kan Nack complex, Kon Tum Massif, Vietnam. J Asian Earth Sci 25(4):653–677

Metcalfe I (1996) Gondwanaland dispersion, Asian accretion and evolution of eastern Tethys. Aust J Earth Sci 43(6):605–623

Metcalfe I (2013) Gondwana dispersion and Asian accretion: tectonic and palaeogeographic evolution of eastern Tethys. J Asian Earth Sci 66:1–33

Miller CF (1985) Are strongly peraluminous magmas derived from pelitic sedimentary sources. J Geol 93(6):673–689

Nakakuki T, Mura E (2013) Dynamics of slab rollback and induced back-arc basin formation. Earth Planet Sci Lett 361:287–297

Nakano N, Osanai Y, Minh NT, Miyamoto T, Hayasaka Y, Owada M (2008) Discovery of high-pressure granulite-facies metamorphism in northern Vietnam: constraints on the Permo-Triassic Indochinese continental collision tectonics. Comptes Rendus Geosci 340(2–3):127–138

Nakano N, Osanai Y, Sajeev K, Hayasaka Y, Miyamoto T, Minh NT, Owada M, Windley B (2010) Triassic eclogite from northern Vietnam: inferences and geological significance. J Metamorph Geol 28(1):59–76

Nam TN, Toriumi M, Itaya T (1998) P–T–t paths and post-metamorphic exhumation of the Day Nui Con Voi shear zone in Vietnam. Tectonophysics 290(3–4):299–318

Owada M, Osanai Y, Hokada T, Nakano N (2006) Timing of metamorphism and formation of garnet granite in the Kontum Massif, central Vietnam: evidence from monazite EMP dating. J Mineral Petrol Sci 101(6):324–328

Peng TP, Fan WM, Zhao GC, Peng BX, Xia XP, Mao YS (2015) Petrogenesis of the early Paleozoic strongly peraluminous granites in the Western South China Block and its tectonic implications. J Asian Earth Sci 98:399–420

Qi XX, Zhao YH, Zhu LH, Li ZQ (2012) Discovery of high-pressure pelitic granulite in Ailaoshan orogenic belt, southeastern Tibet, and its tectonic implications. Acta Petrol Sin 28(6):1846–1856 **(in Chinese with English abstract)**

Qi XX, Santosh M, Zhu LH, Zhao YH, Hu ZC, Zhang C, Ji FB (2014) Mid-Neoproterozoic arc magmatism in the northeastern margin of the Indochina block, SW China: geochronological and petrogenetic constraints and implications for Gondwana assembly. Precambrian Res 245:207–224

Rapp RP, Watson EB (1995) Dehydration melting of metabasalt at 8-32-kbar-implications for continental growth and crust-mantle recycling. J Petrol 36(4):891–931

Roberts MP, Clemens JD (1993) Origin of high-potassium, calc-alkaline, I-type granitoids. Geology 21(9):825–828

Roger F, Arnaud N, Gilder S, Tapponnier P, Jolivet M, Brunel M, Malavieille J, Xu ZQ, Yang JS (2003) Geochronological and geochemical constraints on Mesozoic suturing in east central Tibet. Tectonics 22(4):1–20

Roger F, Maluski H, Leyreloup A, Lepvrier C, Thi PT (2007) U–Pb dating of high temperature metamorphic episodes in the Kon Tum Massif (Vietnam). J Asian Earth Sci 30(3–4):565–572

Roger F, Maluski H, Lepvrier C, Van TV, Paquette JL (2012) LA-ICPMS zircons U/Pb dating of Permo-Triassic and Cretaceous magmatisms in Northern Vietnam—geodynamical implications. J Asian Earth Sci 48(2012):72–82

Roger F, Jolivet M, Maluski H, Respaut JP, Munch P, Paquette JL, Van TV, Van VN (2014) Emplacement and cooling of the Dien Bien Phu granitic complex: implications for the tectonic evolution of the Dien Bien Phu Fault (Truong Son Belt, NW Vietnam). Gondwana Res 26(2):785–801

Schoonmaker A, Kidd WSF, Bradley DC (2005) Foreland-forearc collisional granitoid and mafic magmatism caused by lower-plate lithospheric slab breakoff: the Acadian of Maine, and other orogens. Geology 33(12):961–964

Shen SY, Wei QR, Cheng HL, Mo XX (1998) Metamorphic peridotite and rock series of ophiolite belt in Mt. Ailao, Yunnan Province. Chin Sci Bull 43(11):955–958

Soderlund U, Patchett JP, Vervoort JD, Isachsen CE (2004) The Lu-176 decay constant determined by Lu–Hf and U–Pb isotope systematics of Precambrian mafic intrusions. Earth Planet Sci Lett 219(3–4):311–324

Sone M, Metcalfe I (2008) Parallel Tethyan sutures in mainland Southeast Asia: new insights for Palaeo-Tethys closure and implications for the Indosinian orogeny. Comptes Rendus Geosci 340(2–3):166–179

Sun SS, McDonough WF (1989) Chemical and isotopic systematics of oceanic basalts: implication for mantle composition and process. Geol Soc Lond Spec Publ 42(S1):313–345

Tang GJ, Wyman DA, Wang Q, Li J, Li ZX, Zhao ZH, Sun WD (2012) Asthenosphere-lithosphere interaction triggered by a slab window during ridge subduction: trace element and Sr–Nd–Hf–Os isotopic evidence from Late Carboniferous tholeiites in the western Junggar area (NW China). Earth Planet Sci Lett 329(2012):84–96

Thompson AB, Connolly JAD (1995) Melting of the continental-crust—some thermal and petrological constraints on anatexis in continental collision zones and other tectonic settings. J Geophys Res Solid Earth 100(B8):15565–15579

Tian LY, Castillo PR, Hilton DR, Hawkins JW, Hanan BB, Pietruszka AJ (2011) Major and trace element and Sr–Nd isotope signatures of the northern Lau Basin lavas: implications for the composition and dynamics of the back-arc basin mantle. J Geophys Res Solid Earth 116(B11201):1–18

Usuki T, Lan CY, Wang KL, Chiu HY (2013) Linking the Indochina block and Gondwana during the Early Paleozoic: evidence from U–Pb ages and Hf isotopes of detrital zircons. Tectonophysics 586:145–159

Wang CY, Zhou MF, Sun Y, Arndt NT (2012) Differentiation, crustal contamination and emplacement of magmas in the formation of the Nantianwan mafic intrusion of the similar to 260 Ma Emeishan large igneous province, SW China. Contrib Mineral Petrol 164(2):281–301

Wang YJ, Fan WM, Zhang GW, Zhang YH (2013) Phanerozoic tectonics of the South China Block: key observations and controversies. Gondwana Res 23(4):1273–1305

Wang QF, Deng J, Li CS, Li GJ, Yu L, Qiao L (2014) The boundary between the Simao and Yangtze blocks and their locations in Gondwana and Rodinia: constraints from detrital and inherited zircons. Gondwana Res 26(2):438–448

Wang YJ, Zhou YZ, Liu HC, Cai YF (under review) Neoproterozoic subduction along the SW Yangtze Block: Geochrogological and geochemical evidence from the Ailaoshan granitic and migmatite rocks. Precambrian Res

Wiedenbeck M, Alle P, Corfu F, Griffin WL, Meier M, Oberli F, Von Quadt A, Roddick JC, Speigel W (1995) Three natural zircon standards for U–Th–Pb, Lu–Hf, trace-element and REE analyses. Geostand Newslett 19:1–23

Wu YB, Zheng YF (2004) Genesis of zircon and its constraints on interpretation of U–Pb age. Chin Sci Bull 49(15):1554–1569

Wu FY, Yang YH, Xie LW, Yang JH, Xu P (2006) Hf isotopic compositions of the standard zircons and baddeleyites used in U–Pb geochronology. Chem Geol 234(1–2):105–126

Xu JF, Castillo PR (2004) Geochemical and Nd-Pb isotopic characteristics of the Tethyan asthenosphere: implications for the origin of the Indian Ocean mantle domain. Tectonophysics 393(1–4):9–27

Xu PF, Sun RM, Liu FT, Wang QC, Cong BL (2000) Seismic tomography showing subduction and slab breakoff of the Yangtze block beneath the Dabie-Sulu orogenic belt. Chin Sci Bull 45(1):70–74

Xu YG, Chung SL, Jahn BM, Wu GY (2001) Petrologic and geochemical constraints on the petrogenesis of Permian-Triassic Emeishan flood basalts in southwestern China. Lithos 58(3–4):145–168

Yang JH, Wu FY, Shao JA, Wilde SA, Xie LW, Liu XM (2006) Constraints on the timing of uplift of the Yanshan fold and thrust belt, North China. Earth Planet Sci Lett 246(3–4):336–352

Yang YH, Zhang HF, Xie LW, Wu FY (2007) Accurate measurement of neodymium isotopic composition using neptune multiple collector inductively coupled plasma mass spectrometry. Chin J Anal Chem 1(35):71–74 **(in Chinese with English abstract)**

Yang TN, Ding Y, Zhang HR, Fan JW, Liang MJ, Wang XH (2014) Two-phase subduction and subsequent collision defines the

Paleotethyan tectonics of the southeastern Tibetan Plateau: evidence from zircon U–Pb dating, geochemistry, and structural geology of the Sanjiang orogenic belt, southwest China. Geol Soc Am Bull 126(11–12):1654–1682

Yuan HL, Gao S, Liu XM, Li HM, Gunther D, Wu FY (2004) Accurate U–Pb age and trace element determinations of zircon by laser ablation-inductively coupled plasma-mass spectrometry. Geostand Geoanal Res 28(3):353–370

YunnanBGMR (1990) Regional geology of yunnan province. Geology Publishing House, Beijing, pp 273–428 **(in Chinese)**

Zen EA (1986) Aluminum enrichment in silicate melts by fractional crystallization—some mineralogic and petrographic constraints. J Petrol 27(5):1095–1117

Zhang ZC, Mahoney JJ, Mao JW, Wang FH (2006) Geochemistry of picritic and associated basalt flows of the western Emeishan flood basalt province, China. J Petrol 47(10):1997–2019

Zhang WP, Wang LQ, Wang BD, Wang DB, Dai J, Liu W (2011) Chronology, geochemistry and petrogenesis of Deqin granodiorite body in the middle section of Jiangda-Weixi arc. Acta Petrol Sin 27(9):2577–2590

Zhang RY, Lo CH, Chung SL, Grove M, Omori S, Iizuka Y, Liou JG, Tri TV (2013) Origin and tectonic implication of ophiolite and eclogite in the Song Ma Suture Zone between the South China and Indochina Blocks. J Metamorph Geol 31(1):49–62

Zhang KJ, Xia B, Zhang YX, Liu WL, Zeng L, Li JF, Xu LF (2014a) Central Tibetan Meso-Tethyan oceanic plateau. Lithos 210:278–288

Zhang RY, Lo CH, Li XH, Chung SL, Anh TT, Tri TT (2014b) U–Pb dating and tectonic implication of ophiolite and metabasite from the Song Ma suture zone, northern Vietnam. Am J Sci 314(2):649–678

Zhong DL (1998) The Paleotethysides in West Yunnan and Sichuan. Science Press, Beijing, pp 1–230 **(in Chinese)**

Zhu JJ, Hu RZ, Bi XW, Zhong H, Chen H (2011) Zircon U–Pb ages, Hf–O isotopes and whole-rock Sr–Nd–Pb isotopic geochemistry of granitoids in the Jinshajiang suture zone, SW China: constraints on petrogenesis and tectonic evolution of the Paleo-Tethys Ocean. Lithos 126(3–4):248–264

Zi JW, Fan WM, Wang YJ, Cawood PA, Peng TP, Sun LH, Xu ZQ (2010) U–Pb geochronology and geochemistry of the Dashibao basalts in the Songpan-Ganzi Terrane, SW China, with implications for the age of Emeishan volcanism. Am J Sci 310(9):1054–1080

Zi JW, Cawood PA, Fan WM, Tohver E, Wang YJ, McCuaig TC (2012a) Generation of early Indosinian enriched mantle-derived granitoid pluton in the Sanjiang Orogen (SW China) in response to closure of the Paleo-Tethys. Lithos 140(2012):166–182

Zi JW, Cawood PA, Fan WM, Wang YJ, Tohver E (2012b) Contrasting rift and subduction-related plagiogranites in the Jinshajiang ophiolitic melange, southwest China, and implications for the Paleo-Tethys. Tectonics 31(2):1–18

Zi JW, Cawood PA, Fan WM, Wang YJ, Tohver E, McCuaig TC, Peng TP (2012c) Triassic collision in the Paleo-Tethys Ocean constrained by volcanic activity in SW China. Lithos 144(2012):145–160

Zi JW, Cawood PA, Fan WM, Tohver E, Wang YJ, McCuaig TC, Peng TP (2013) Late Permian-Triassic magmatic evolution in the Jinshajiang orogenic belt, SW China and implications for orogenic processes following closure of the Paleo-Tethys. Am J Sci 313(2):81–112